Air Injection in Water with Different Nozzles

Iran E. Lima Neto[1]; David Z. Zhu, M.ASCE[2]; and Nallamuthu Rajaratnam, F.ASCE[3]

Abstract: Air injection systems have a wide range of environmental engineering applications. In this study, we conducted experiments on air injection in a relatively large water tank to investigate the effect of nozzle type, including single/multiple orifice nozzles and a porous airstone, on the characteristics of the bubbles and the induced flow structure. Measurements of bubble characteristics and flow field surrounding the bubble core were obtained using a double-tip optical probe and particle image velocimetry, respectively. The results revealed that bubble velocity did not change significantly with different nozzles, but bubble size decreased significantly while interfacial area, liquid entrainment rate, and kinetic energy of the mean and turbulent flow increased significantly by using the porous airstone instead of nozzles with large orifices. The results for a nozzle with multiple orifices of small diameter are comparable to those for the airstone, which suggests the suitability of its use for systems susceptible to clogging of the pores. Correlations using adequate length and velocity scales are also proposed to describe both bubble and liquid flow characteristics. Finally, applications of the results for different artificial aeration/mixing systems are presented.

DOI: 10.1061/(ASCE)0733-9372(2008)134:4(283)

CE Database subject headings: Aeration; Turbulent flow; Air injection.

Introduction

Bubble plumes are widely used for artificial aeration and mixing in lakes, reservoirs, and wastewater treatment systems (Wüest et al. 1992; McCord et al. 2000; McGinnis and Little 2002; DeMoyer et al. 2003; McGinnis et al. 2004; Sahoo and Luketina 2006). These types of two-phase flows are formed when air or pure oxygen is continuously discharged into the water, producing bubbles that rise inducing surrounding liquid entrainment and oxygen transfer to the water. The size of the rising bubbles depends on bubble breakup/coalescence processes (which depend on several factors such as turbulence, bubble collision frequency, presence of impurities, and so forth) and the counterbalancing effects of mass transfer and reducing pressure head acting on the bubble surface. Two important parameters that are controlled by the sizes of the bubbles are the mass transfer coefficient or liquid film coefficient, K_L, and the air-water interfacial area per unit liquid volume or specific interfacial area, a. These parameters are related to the rate of oxygen transfer to the water through the following equation, derived from Fick's law of diffusion (Mueller et al. 2002)

$$\frac{dC}{dt} = K_L a(C_s - C) \tag{1}$$

where C=dissolved oxygen (DO) concentration in the water; and C_s=saturation DO concentration. Correction factors for K_L and C_s to account for the effects of water temperature, pressure, and presence of impurities are commonly used in wastewater aeration systems (see Mueller et al. 2002). While the mass transfer coefficient K_L increases with bubble diameter, reaching a maximum of approximately 0.05 cm/s for bubbles of about 2 mm and then decreasing as the diameter increases (Barnhart 1969; Montarjemi and Jameson 1978), the specific interfacial area a decreases significantly as the mean bubble diameter increases. The sizes of the bubbles also determine their shape and velocity (Clift et al. 1978), which in return affect their residence time in the water and, as a consequence, the rate of oxygen transfer to the water. An experimental study conducted by Leitch and Baines (1989) on dilute bubble plumes also showed that bubble size affects the surrounding flow structure because the individual bubble wakes play an important role in the liquid entrainment rate. Additional liquid turbulence caused by the wakes of the bubbles and bubble collision processes has also been observed recently by Brücker and Schröder (2004).

In artificial aeration systems, oxygen transfer to the water also occurs during bubble formation at the orifices and bubble bursting at the free surface. In principle, the oxygen transfer rate for each of these processes could also be described as a function of a mass transfer coefficient, interfacial area, and DO concentration deficit (Eckenfelder 1959; Barnhart 1969), as mentioned above for rising bubbles [see Eq. (1)]. However, the complexity of these processes makes the estimation of the mass transfer coefficient and interfacial area very difficult. Following the methods of McWhirter and Hutter (1989) and DeMoyer et al. (2003), Schierholz et al. (2006) used measurements of DO concentrations in several aeration tanks of different scales and performed a regression analysis to separate the contributions of oxygen transfer to the water from the bubbles and across the air-water surface. They reported that for

[1]Ph.D. Candidate, Dept. of Civil and Environmental Engineering, Univ. of Alberta, Edmonton AB, Canada T6G 2W2. E-mail: limaneto@ualberta.ca

[2]Professor, Dept. of Civil and Environmental Engineering, Univ. of Alberta, Edmonton AB, Canada T6G 2W2 (corresponding author). E-mail: david.zhu@ualberta.ca

[3]Professor Emeritus, Dept. of Civil and Environmental Engineering, Univ. of Alberta, Edmonton AB, Canada T6G 2W2. E-mail: nrajaratnam@ualberta.ca

Note. Discussion open until September 1, 2008. Separate discussions must be submitted for individual papers. To extend the closing date by one month, a written request must be filed with the ASCE Managing Editor. The manuscript for this paper was submitted for review and possible publication on October 25, 2006; approved on October 8, 2007. This paper is part of the ***Journal of Environmental Engineering***, Vol. 134, No. 4, April 1, 2008. ©ASCE, ISSN 0733-9372/2008/4-283–294/$25.00.

relatively high air flow rates, fine bubble diffusers are better for bubble aeration while coarse bubble diffusers are more suitable for surface aeration. They also proposed correlations for bubble and surface volumetric mass transfer coefficients (K_La). A summary of standard measurement methods to estimate the total value of K_La through regression analysis in aeration systems is given in a recent ASCE standard-ASCE/EWRI 2-06 (ASCE 2007). On the other hand, in the case of point-source bubble plumes in lakes or reservoirs with much larger free surface areas, additional oxygen transfer will occur through turbulent diffusion at the water surface due to the effects of circulation water flow and wind stream (see McCord et al. 2000). Several equations of K_L for each of these effects are summarized by Chu and Jirka (2003) and Lima Neto et al. (2007b).

Sufficient circulation and mixing is also required in artificial aeration systems to disperse DO and provide uniform organic matter concentrations throughout the water. Due to the difficulty in measuring flow patterns for a particular aeration system, limited information on circulation and mixing characteristics is available and usually a velocity of about 0.15 m/s across the basin bottom is assumed to prevent solids deposition in degritted wastewater tanks (WPCF 1988; Mueller et al. 2002). Soga and Rehmann (2004), Wain and Rehmann (2005) and García and García (2006) recently conducted measurements of turbulence in the flow field surrounding a bubble plume for aeration and mixing in a wastewater tank to prevent anaerobic conditions. These measurements will help to evaluate the mixing requirements and associated transport processes induced by a bubble plume.

Despite the importance of bubble properties and mean/turbulent liquid flow structure on the performance of aeration/mixing systems and their designs, very few studies have been devoted to this issue. In addition to bulk dissolved oxygen measurements, Rosso and Stenstrom (2006) roughly estimated average bubble size and velocity in a relatively small aeration tank (with diameter smaller than 40 cm), but no detailed information such as bubble size distribution, bubble slip velocity, interfacial area, and liquid flow structure were provided. The studies mentioned above were conducted for diffusers occupying a large area on the bottom of the tank (partial or total floor coverage). The case of point source discharges have been studied by Kobus (1968), Iguchi et al. (1989, 1992), Swan and Moros (1993), Friedl and Fanneløp (2000), Soga and Rehmann (2004), Wain and Rehmann (2005), and García and García (2006). Among these studies, only Iguchi et al. (1989, 1992) investigated the effect of the single orifice nozzle diameter on bubble properties and mean/turbulent liquid flow structure. However, their experiments were conducted in small scale vessels (or confined setups) where the flow behaves differently from unbounded bubble plumes (see Lima Neto et al. 2007a).

The present investigation was similar to Iguchi's, however, it was conducted in a much larger water tank, with the bubble plumes away from the boundaries. Multiple orifice nozzles and a porous airstone were also tested in addition to single orifice nozzles. Therefore, the aim of this work was to investigate experimentally the effect of nozzle type on the characteristics of the bubbles such as bubble size, velocity, and interfacial area as well as the mean/turbulent liquid flow structure generated in a relatively large water tank. The results of this study are applicable to shallow water cases such as artificial aeration/mixing in wastewater tanks (Mueller et al. 2002) and rivers (Lima Neto et al. 2007b) and provide information for initial conditions in bubble plume models.

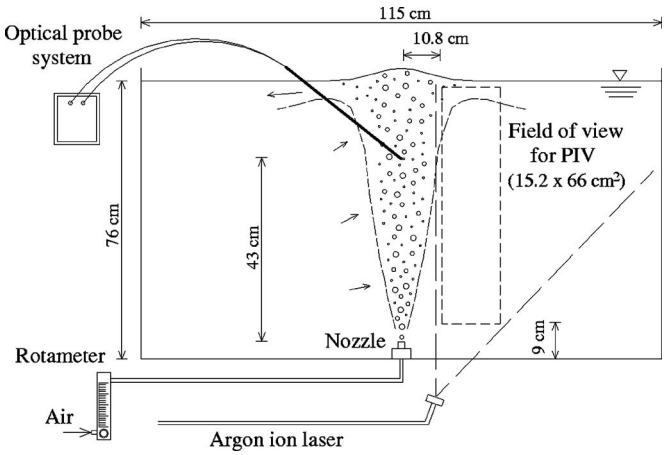

Fig. 1. Schematic of experimental apparatus

Experimental Apparatus and Program

The experiments were performed in a square glass-walled tank of 1.2 m with a height of 0.8 m, shown schematically in Fig. 1. The tank was filled with tap water at $20\pm1\,^{\circ}C$ up to a depth of 0.76 m. The gas supply was taken from an air line with 1.0 atm pressure and temperature of $21\pm1\,^{\circ}C$. Volumetric air flow rates, Q_a, of 33.3 and 50.0 cm^3/s were adjusted by a rotameter and discharged through different nozzles (single/multiple orifice nozzles and a porous airstone), connected by a poly vinyl chloride (PVC) pipe with inner diameter of 2.54 cm. These air flow rates were chosen because preliminary dye injection tests showed that for smaller values (Q_a=16.7 cm^3/s), the flow behaves like weak bubble plumes with the entrained liquid spreading approximately with the square root of height, while for higher values (Q_a=33.3 and 50.0 cm^3/s), the entrained liquid spreads linearly with height, as expected for larger-scale bubble plumes (see Leitch and Baines 1989). Higher air flow rates (Q_a=66.7 cm^3/s) were not considered here because the flow became very unstable with strong surface waves being reflected from the walls of the tank. As sketched in Fig. 2, the single/multiple orifice nozzles were built from PVC caps where circular holes of different sizes were drilled, while the porous nozzle was built by drilling a circular hole of 6 mm diameter on a PVC cap and gluing a porous airstone on its top. The nozzles of 1×3.0, 4×1.5, and 9×1.0 mm were designed such that the total orifice area remains the same, the single-orifice nozzle of 0.6 mm and the porous airstone being special cases. The sizes of the orifices used here were similar to those usually employed in fine and intermediate bubble diffuser systems, which range from about 0.1 to 5.0 mm (Mueller et al. 2002). The nozzles were placed at the center of the tank and their exit was about 4.5 cm above the bottom. Experiments with each

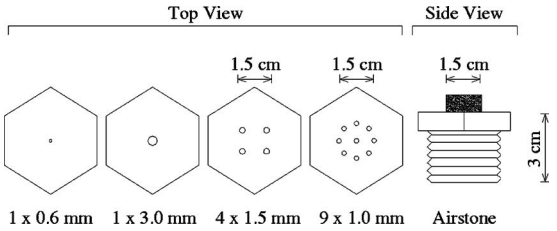

Fig. 2. Sketch of nozzle types, indicating number and diameter of orifices (top view) and porous airstone nozzle (side view)

Table 1. Estimated Volumetric Mass Transfer Coefficients (K_La) for Each Experimental Condition. Values of K_L were Obtained from Correlation Given by Wüest et al. (1992) and McGinnis and Little (2002) as Function of Mean Bubble Diameter

	Estimated values of K_La (h^{-1})	
Nozzle	Q_a=33.3 cm^3/s	Q_a=50.0 cm^3/s
1×0.6 mm	12.34	15.91
1×3.0 mm	8.65	11.77
4×1.5 mm	11.04	13.83
9×1.0 mm	13.88	15.79
Airstone	18.96	19.16

nozzle and flow rate (see Table 1) were performed separately for optical probe tests and particle image velocimetry (PIV) tests, which are described in the following sections.

Optical Probe Tests

In the study, a double-tip optical fiber probe system (RBI Instrumentation) was used to measure bubble characteristics. The system is described as follows: A module emits infrared light via two fiber-optic cables to the tips of the probe, 2 mm apart. Each tip extends 1.5 cm and is sharpened into 30 μm diameter. Emitted light is refracted when water surrounds the tips, and reflected back to the module when air surrounds the tips. The reflected light passes through a semitransparent mirror combined with a prism towards a photosensitive diode in the module, and can be recorded at a sampling rate of 1 MHz. Finally, direct amplification and detection through a threshold technique results in a two-state signal corresponding to the phase (air or water) surrounding the tips. Thus, the double-tip optical fiber probe can measure not only void fraction and bubble frequency but also estimate through cross correlation the velocity in which a bubble travels from one tip to the other. Similar RBI double-tip optical fiber probe systems were used by Rensen and Roig (2001), Boes and Hager (2003), Kiambi et al. (2003), Chaumat et al. (2005), and Murzyn et al. (2005) to measure two-phase flow characteristics in bubbly flows.

The optical probe signals were processed to calculate void fraction (α), bubble frequency (f_b), and velocity (u_b) and the following equations given by Chanson (1997) and Toombes and Chanson (2005) were used to estimate the specific interfacial area (a) and bubble mean Sauter diameter (d_b)

$$a = 4f_b/u_b \tag{2}$$

$$d_b = 6\alpha/a \tag{3}$$

Since Eqs. (2) and (3) assume that the bubbles are spherical and their motion is unidirectional, which does not often occur in artificial aeration/mixing systems, we conducted two preliminary tests to verify the accuracy of the optical probe measurements. The first test was performed in a bubble column of 5 cm diameter filled with tap water up to 68 cm, as shown schematically in Fig. 3. Air was injected from the bottom at different flow rates through the porous airstone, and the void fraction was obtained using the optical probe with the additional water level due to the presence of the bubbles also considered (see Chang et al. 2003). The results showed that the optical probe underestimates the void fraction by about 11%, which is in agreement with the differences of up to 14% obtained by Kiambi et al. (2003) by comparing double optical probe measurements and image processing. The second test

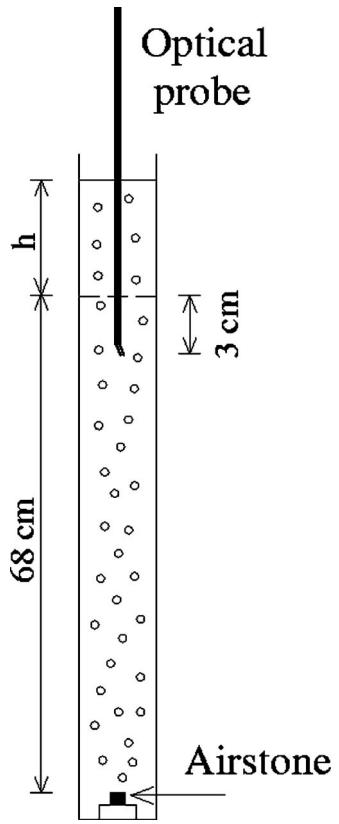

Fig. 3. Bubble column tests to validate measurements of void fraction

was performed in the tank (see Fig. 1) where air was injected at low flow rates through different nozzles to produce dilute bubble plumes containing bubbles ranging from about 2 to 10 mm volume-equivalent sphere diameter. In this case the optical probe was placed in the horizontal position with the tips 2 mm apart in the vertical direction to measure both bubble rising velocity and size. Images of these bubbles were then acquired using a high resolution charge coupled device (CCD) camera (TM-1040, Pulnix America Inc.) controlled by a computer frame grabber system (Streams 5, IO Industries Inc.) with a frame rate of 30 frames/s and exposure time of 1/4,000 s. The results showed that the optical probes overestimate the bubble velocity by about 29% and underestimate the bubble size by about 10%. Similar results were obtained by Chaumat et al. (2005), who tested vertical bubbly flows with bubble size ranging from about 6 to 9 mm and obtained overestimations of bubble velocity of up to 32% and underestimations of bubble size of up to 20%.

Additional preliminary tests conducted in the tank with Q_a equal to 33.3 and 50.0 cm^3/s clearly showed a low-frequency lateral oscillation of the bubble core of about ±5°. This nonstationary nature of the flow, usually called wandering motion, persisted even for long-time observations (>3 h) and it was attributed to buoyancy driven instabilities enhanced by the presence of the tank walls. Similar instabilities were previously reported in bubble plume experiments (Leitch and Baines 1989; Fanneløp et al. 1991; García and García 2006). In order to obtain stable measurements, tests were performed for sampling times ranging from 2 to 30 min. The results showed that 5 min was enough to obtain measurements of bubble characteristics within less than about ±10% difference. Therefore, all the bubble plume experiments were performed for 5 min duration. The measurements were

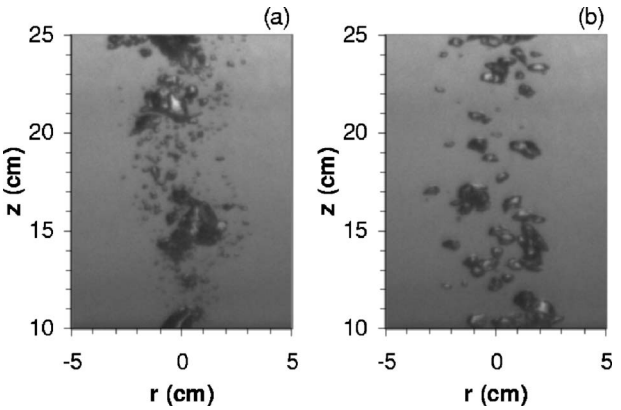

Fig. 4. Typical images of bubbles for Q_a=50.0 cm^3/s: (a) single orifice nozzle of 0.6 mm (showing breakup of large bubbles into smaller bubbles); (b) multiple orifice nozzle of 9×1.0 mm (showing almost no bubble breakup)

taken for radial distances from the plume centerline r of 0, 2, 4, and 6 cm and at a height above the nozzle exit z of 43 cm, which was far enough for bubble breakup/coalescence processes to be completed. The measurements were taken 5 min after start of air injection in the tank and the time interval between successive experiments was at least 20 min to ensure that the motion induced in the preceding experiment ceased completely. Fig. 4 shows typical images of the bubbles in which bubble breakup occurs from approximately 10 to 25 cm above the nozzle exit. Bubble breakup processes were more evident for single orifice nozzles, where larger irregular bubbles were formed close to the nozzle exit due to coalescence and collapsed into much smaller spherical and ellipsoidal bubbles due to velocity gradients and turbulence. This is in contrast to the tests with multiple orifice nozzles and the airstone, where most bubbles formed at the nozzle exit were ellipsoidal and with approximately the same size.

PIV Tests

The time criteria used for the optical probe tests were also applied for the PIV tests. In these tests, silver-coated glass particles with a density of 1.65 g/cm^3 and a mean diameter of 15 μm were homogenously distributed over the tank. A continuous 6 W argon ion laser operating at 488 nm (Stabilite 2017, Spectra-Physics Lasers) connected by a fiber-optic cable to a cylindrical lens (OZ Optics Ltd.) illuminated a field of view of 15.2×66 cm^2, 4.5 cm above the nozzle exit and 10.8 cm from the nozzle centerline (see Fig. 1). A high resolution CCD camera (Pulnix TM-1040) controlled by a computer frame grabber system (Streams 5, I. O. Industries Inc.) captured images of the particles with a frame rate of 30 frames/s and exposure time of 1/60 s. The field of view corresponded to an image size of 240×1,040 pixels, yielding a resolution of 15.8 pixels/cm. The displacements between subsequent images were computed using a standard cross-correlation PIV algorithm (Heurisko, version 4.0.8, Aeon Verlag and Studio) with an interrogation window size of 64×64 pixels and 50% overlap between adjacent windows.

Because of the nonstationary nature of the flow mentioned above, a digital filtering technique was used to separate the turbulent motions (i.e., high-frequency signals) and the periodic motions (i.e., low-frequency signals) from the original velocity signals, and the mean/turbulent velocity components at each point were then computed using a computer algorithm written in Matlab (The Mathworks Inc.).

Measurements of the flow field within the bubble core were not possible with PIV because the bubbles were much bigger and brighter than the tracer particles and the intensity of the light reflected from them saturated the camera and corrupted the results. However, an electromagnetic propeller anemometer (Omni Instruments, MiniWater20) with internal diameter and casing of 22 and 28 mm, respectively, was used to measure mean vertical water velocity inside the bubble core. The anemometer is suitable for velocities higher than 2 cm/s with an accuracy of 2%. These measurements were taken when the bubble plumes were in a straight vertical position and were used to estimate the relative velocity between the bubbles and the water (i.e., bubble slip velocity). Similar propeller anemometers have been used in bubble plume studies by Swan and Moros (1993), Riess and Fanneløp (1998), and Friedl and Fanneløp (2000).

It is important to stress that both optical probe and PIV tests were performed on tap water with negligible suspended solids concentration. However, if a relatively large amount of suspended solids is added to the water, the refractive index of the mixture will be close to that of the air phase and corrupt the optical probe measurements (see Boyer et al. 2002). The presence of suspended solids in the water will also affect the PIV measurements. The images of suspended solids need to be separated from those of tracer particles either by using fluorescent tracer particles or by size and geometry separation (see Kiger and Pan 2000). Note that in our PIV tests, the weight concentration of tracer particles was so small (less than 0.001%) that their interactions with the bubbles were considered negligible.

Experimental Results and Analysis

Bubble Characteristics

The time series of void fraction indicated a low-frequency periodic fluctuation about the mean value of about 0.03 Hz, corresponding approximately to the lateral oscillation of the bubble core. Fig. 5 shows typical void fraction time series measured with the two fiber-optic tips of the RBI probe. The time-averaged radial distributions of all void fraction (and bubble frequency) measurements followed Gaussian curves similar to those obtained by Swan and Moros (1993) and Friedl and Fanneløp (2000). Our discussion will focus, however, on the time-averaged radial distributions of bubble mean Sauter diameter, velocity, and specific interfacial area, which are considered of major importance in artificial aeration systems. Fig. 6 shows typical bubble size distributions obtained from measurements at the plume centerline. These distributions resemble gamma or log-normal curves with more uniform bubble sizes (narrower band) as the number of orifices increases and their size decreases. Fig. 7 shows typical radial distributions of mean Sauter diameter, velocity, and specific interfacial area. It can be seen that while the bubble mean Sauter diameter and velocity distributions are well described by a straight line, the specific interfacial area distribution follows a Gaussian curve.

As the bubble velocity is the combination of the water velocity and the bubble slip velocity, the water velocity within the plume was measured using the Omni anemometer. Fig. 7(b) shows that the water velocity decreased linearly from the maximum at the center of the plume to close to zero at the edge of the plume. In

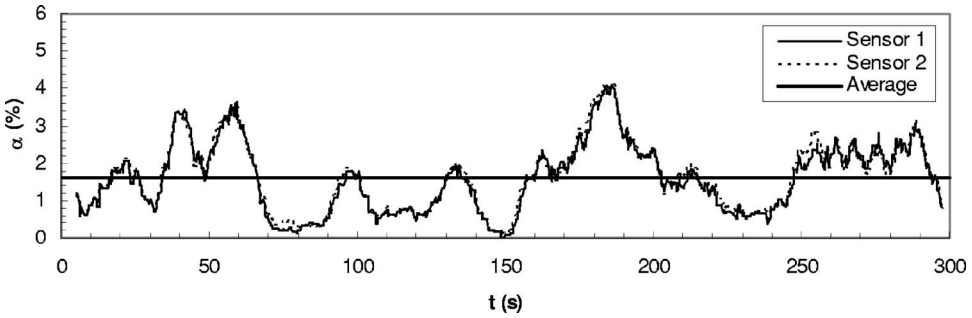

Fig. 5. Typical void fraction time series for two fiber-optic tips of RBI probe: measurements taken at r=2 cm and z=43 cm (nozzle type: 4×1.5 mm, Q_a=50.0 cm^3/s)

addition, the bubble slip velocity was about 0.55 m/s, which is higher than the terminal bubble velocity of about 0.30 m/s given by Clift et al. (1978) for isolated bubbles of similar diameters. This may be because trailing bubbles in the wake of leading bubbles rise faster than isolated bubbles due to drag reduction, as observed by Ruzicka (2000). These measurements are important because bubble plume models accounting for oxygen transfer to the water usually assume uniform distributions (top hat) of bubble characteristics, as well as constant slip velocities equal to the terminal bubble velocities given by Clift et al. (see Wüest et al. 1992).

Fig. 8 summarizes the average radial values of bubble mean Sauter diameter ($\overline{d_b}$), absolute bubble velocity ($\overline{u_b}$), and specific interfacial area ($\overline{a}$) for each experimental condition. It can be seen that bubble mean Sauter diameter could be decreased by about 50% while interfacial area could be increased by about 90% by using the porous airstone instead of the single orifice nozzle of 3.0 mm. On the other hand, absolute bubble velocity did not change significantly, as observed by Iguchi et al. (1989, 1992) in a confined bubble plume setup. However, their values were about 30% smaller than those obtained here for similar air flow rates and orifice diameters. This may be attributed to smaller bubbles due to stronger breakup processes in their confined setup as well as lower liquid entrainment rate, which will be discussed further in this paper. The results of bubble mean Sauter diameter and interfacial area for the multiple orifice nozzle of 9×1.0 mm are comparable to those for the airstone. This means that for systems susceptible to rapid clogging, such as porous nozzles in wastewater treatment tanks and natural water bodies with high concentra-

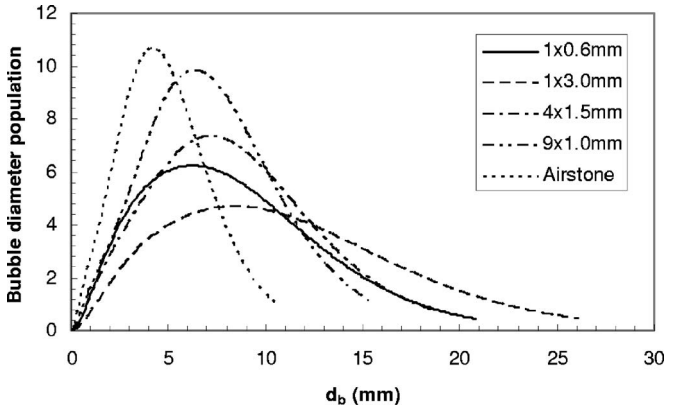

Fig. 6. Typical bubble size distributions obtained from measurements at r=0 cm and z=43 cm (Q_a=33.3 cm^3/s)

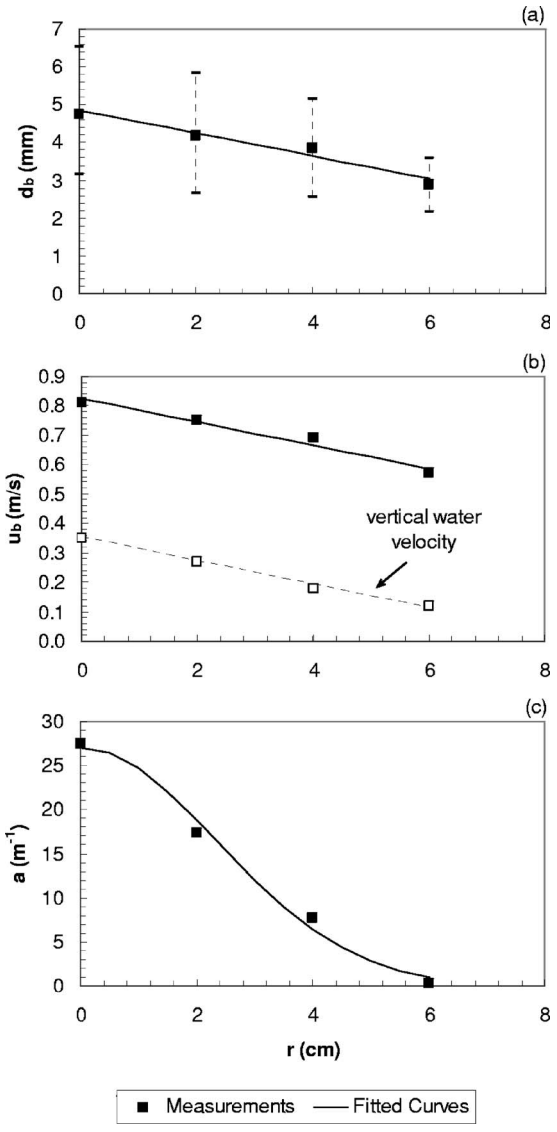

Fig. 7. Typical radial distributions of: (a) bubble mean Sauter diameter (also indicating standard deviations); (b) absolute bubble velocity (also indicating mean vertical water velocity); and (c) specific interfacial area (nozzle type: Airstone, Q_a=33.3 cm^3/s). Measurements shown were taken at z=43 cm.

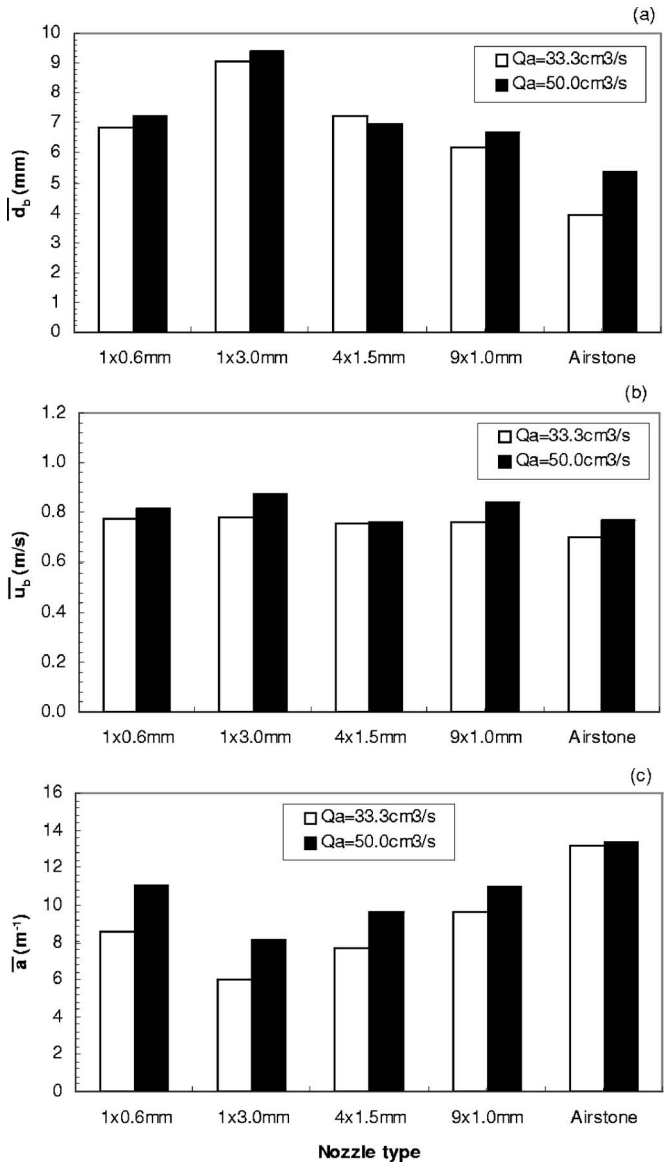

Fig. 8. Average radial values of: (a) bubble mean Sauter diameter; (b) absolute bubble velocity; and (c) specific interfacial area. Measurements shown were taken at $z=43$ cm.

tion of suspended solids and/or organic matter, the use of multiple small-orifice nozzles may be preferable rather than the use of porous airstones. Note that our porous airstone clogged after some tests and needed cleaning to reduce the friction head losses and achieve the desired air flow rates. The results for the single orifice nozzle of 0.6 mm were similar to those of the multiple-orifice nozzle of 9×1.0 mm, but the latter produced bubbles of more uniform size (see Fig. 6). The single orifice nozzle of 0.6 mm presented some advantage over the single orifice nozzle of 3.0 mm and the multiple-orifice nozzle of 4×1.5 mm because the high-velocity jet issuing from its exit produced more bubbles of smaller size due to very strong bubble breakup processes (especially for the higher air flow rate).

In order to normalize the results and make them applicable to other bubble plume conditions, dimensional analysis was conducted. Using the Buckingham's Pi theorem and assuming that the forces due to viscosity, surface tension, and compressibility are negligible compared to the forces due to momentum and buoyancy, under fully turbulent flow conditions in a shallow water tank, the radial distributions of d_b, u_b, and a for a specific height above the nozzle can be described by the following relation

$$\left[\frac{d_b}{L},\frac{u_b}{U},aL\right]=f\left[\frac{r}{L},\mathsf{F}\right] \tag{4}$$

where L=length scale defined by $L=(Q_a^2/g)^{1/5}$; and U=velocity scale defined by $U=Q_a/L^2$. The third parameter F=densimetric Froude number defined by $\mathsf{F}=U_e/\sqrt{d_e g(\rho_w-\rho_a)/\rho_w}$, in which ρ_w and ρ_a=water and air density, respectively, and U_e and d_e=equivalent velocity and diameter for each nozzle, respectively. Since our experiments were conducted for nozzles ranging from single/multiple orifices to a porous airstone, it was not possible to estimate values of U_e and d_e (i.e., F) for each nozzle in order to collapse all the experimental data in one single curve. Therefore, we neglected F and obtained the following dimensionless correlations by adjusting straight lines to the radial distributions of d_b and u_b and a Gaussian curve to the radial distribution of a, the variation corresponding approximately to the upper and lower limits obtained with different nozzles

$$\frac{d_b}{L}=(0.75\pm33\ \%)-0.35\left(\frac{r}{L}\right) \tag{5}$$

$$\frac{u_b}{U}=(2.70\pm11\ \%)-0.13\left(\frac{r}{L}\right) \tag{6}$$

$$aL=(0.23\pm41\ \%)e^{-0.12(r/L)} \tag{7}$$

Fig. 9 shows the adjustment of Eqs. (5)–(7) to experimental data. Not only were good adjustments obtained, but the upper and lower limits represented by dashed lines also clearly show the maximum variation of each parameter with nozzle type (e.g., dimensionless bubble diameter decreases when using the porous airstone instead of the single orifice nozzle of 3.0 mm). This confirms that F is of secondary importance for our sets of experiments.

Surrounding Flow Structure

Similar to void fraction measurements, the liquid velocity time series obtained from PIV measurements also indicated a low-frequency periodic fluctuation about the mean. Fig. 10 shows a typical power spectrum of the horizontal and vertical velocity components, u and v. A line with a slope of $-5/3$ is also shown to indicate the presence of Kolmogorov's inertial subrange. A dominant frequency of about 0.03 Hz was obtained for the velocity signals near the bubble core. Notice that this frequency was the same obtained from void fraction measurements, which implies that the periodic fluctuation of the velocity signals was caused mainly due to the wandering motion (i.e., bubble core oscillation). Because of this nonstationary nature of the flow surrounding the bubble plumes, a digital filtering technique was used to separate the turbulent motions (i.e., high-frequency signals) from the periodic motions (i.e., low-frequency signals). A fixed cutoff frequency of 0.2 Hz was used for all the experimental conditions. This frequency was selected to be higher than the dominant frequency in the spectrum, as described by García and García (2006) and Lima Neto et al. (2007a). Thus, a Butterworth high-pass filter of sixth order was used to eliminate the mean ($\bar{u}$ and $\bar{v}$) and low-frequency periodic (u'' and v'') velocity fluctuations from the original velocity signal and estimate the turbulent (high-

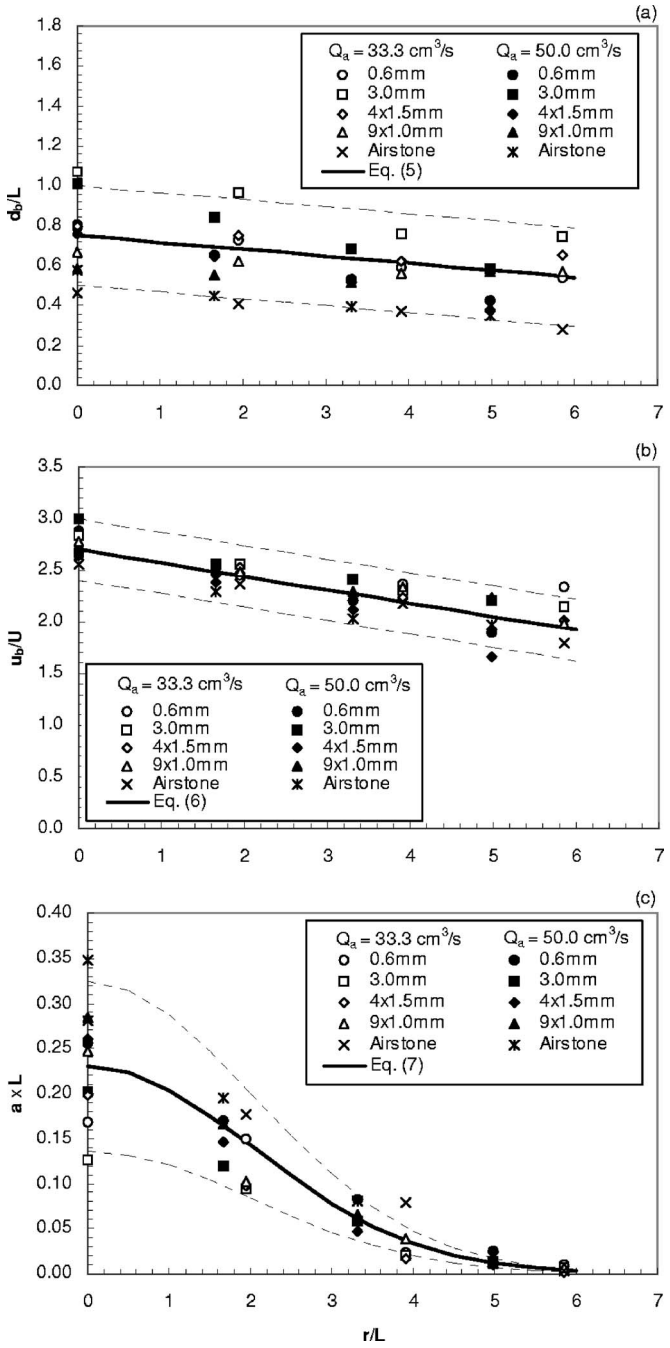

Fig. 9. Adjustment of Eqs. (5)–(7) to experimental data, with dashed lines indicating approximately maximum variation of each parameter with nozzle type

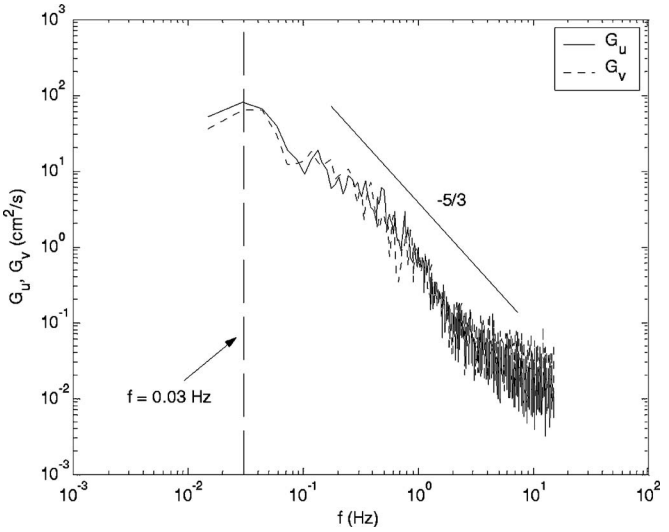

Fig. 10. Power spectrums of horizontal and vertical velocity components (G_u and G_v) measured at r=10.8 cm and z=43 cm indicating dominant frequency (0.03 Hz) and presence of inertial subrange (line with slope of −5/3) (nozzle type: 9×1.0 mm, Q_a=33.3 cm^3/s)

frequency) velocity fluctuations u' and v', where $u=\bar{u}+u'+u''$ and $v=\bar{v}+v'+v''$. An example of this velocity decomposition is shown in Fig. 11. Although the periodic velocity fluctuations were significant, our discussion will focus on the axial distributions of mean/turbulent velocity components near the bubble core, which are important for estimation of the entrainment rate and kinetic energy of the mean/turbulent flow.

A typical time-averaged flow field is shown in Fig. 12. It can be seen that the mean horizontal velocity component, $\bar{u}$, decreases with axial distance from the nozzle while the vertical velocity component, $\bar{v}$, increases until the flow approaches the surface jet region. The initial thickness of the surface jet obtained here was of about 12 cm for all experiments, which is consistent with the thickness of about 1/6 of water depth obtained by Fanneløp et al. (1991) and Riess and Fanneløp (1998) for the flow around line-source bubble plumes. Therefore, the cumulative volumetric entrainment rate, Q_w, was estimated by integrating the product of $\bar{u}$ (measured at r=10.8 cm) by the surface area of a cylinder of radius r_c=10.8 cm surrounding the bubble core from z_1=4.5 cm to z_2=59 cm, where $\bar{u}$ becomes approximately zero and the border of the surface jet region is reached

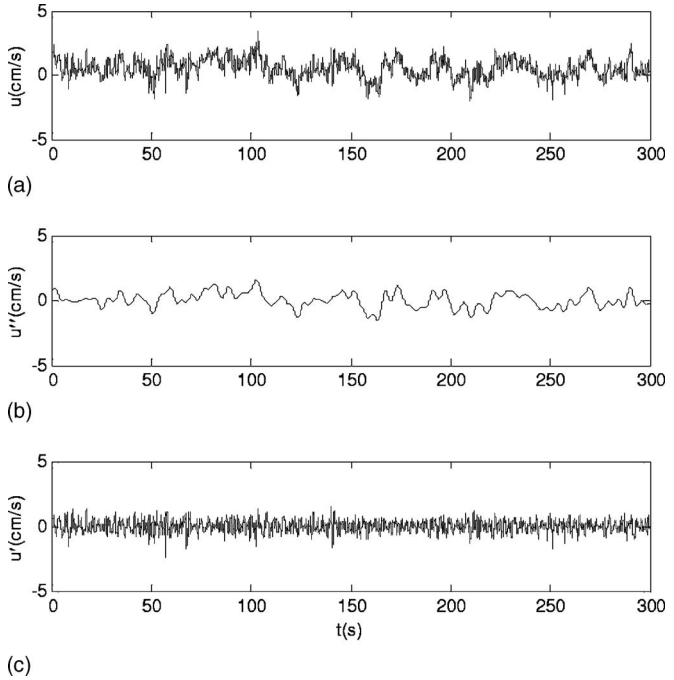

Fig. 11. Velocity decomposition: (a) original velocity signal u measured at r=10.8 cm and z=43 cm; (b) periodic velocity component u''; (c) turbulent velocity component u' (nozzle type: 9×1.0 mm, Q_a=33.3 cm^3/s)

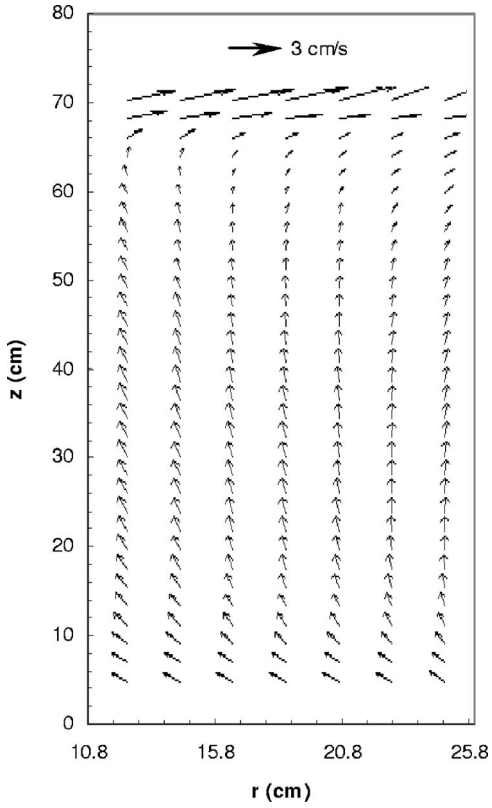

Fig. 12. Time-averaged flow field indicating velocity scale of 3 cm/s (nozzle type: 9×1.0 mm, $Q_a = 33.3$ cm^3/s)

$$Q_w(z) = \int_{z_1}^{z} \bar{u}(z) 2\pi r_c \, dz \tag{8}$$

The kinetic energy of the mean flow (MKE) and turbulent kinetic energy (TKE) were calculated (for measurements at $r = 10.8$ cm) using the following equations

$$\text{MKE} = \tfrac{1}{2}[(\bar{u})^2 + (\bar{v})^2] \tag{9}$$

$$\text{TKE} = \tfrac{1}{2}[\overline{(u')^2} + \overline{(v')^2} + \overline{(w')^2}] \tag{10}$$

Because swirl motion was avoided during the measurements, we assumed that the third mean velocity component $\bar{w}$ was equal to zero in Eq. (9). We also assumed that the third turbulent velocity component w' was equal to v' in Eq. (10). This assumption is supported by measurements of turbulent stresses. Fig. 13 shows typical axial distributions of the turbulent horizontal normal stresses, vertical normal stresses, and shear stresses. It can be seen that the horizontal normal stresses are slightly higher than the vertical normal stresses and that the shear stresses are very small, which implies that the turbulent flow field is nearly isotropic. Therefore, the assumption of $\overline{(w')^2} = \overline{(v')^2}$ is reasonable. The increase in magnitude of the stresses with air flow rate and height is in agreement with the measurements of turbulent kinetic energy, dissipation, and eddy diffusivity obtained, respectively, by García and García (2006), Soga and Rehmann (2004), and Wain and Rehmann (2005) for the flow field surrounding a large-scale bubble plume. Iguchi et al. (1989, 1992) found that the magnitude of the turbulent fluctuations at the bubble core centerline increases with air flow rate but decreases with height in a confined bubble plume setup.

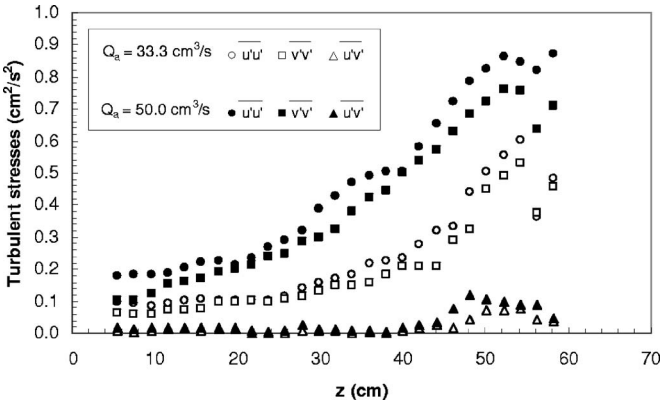

Fig. 13. Typical axial variation of turbulent stresses measured at $r = 10.8$ cm (nozzle type: 9×1.0 mm)

Typical axial distributions of the cumulative entrainment rate and kinetic energy of the mean flow and turbulent kinetic energy are shown in Fig. 14. It can be seen that the variation of Q_w with height is well described by a straight line. Notice that this straight line applies for the region above approximately 10 cm from the nozzle exit, where the bubbles are expected to reach their terminal slip velocity, the flow becomes fully established, and the cumulative entrainment rate increases linearly with height (see Leitch and Baines 1989). The variations of MKE and TKE with height are well described by a polynomial curve and an exponential curve, respectively, but the discrepancy between the measurements of TKE and the exponential curve increases as the flow approaches the surface jet region.

It is important to compare the water flow rate Q_w obtained from the PIV measurements (Fig. 14) with that from the velocity measurements [Fig. 7(b)]. The values of Q_w at 43 cm above the nozzles were obtained by integration of the mean vertical velocities [see Fig. 7(b)], assuming a linear decay of centerline velocity up to about $r = 9$ cm, where the vertical velocity becomes approximately zero. Overall the values of Q_w obtained with direct velocity measurement within the plume were approximately 10% larger than those measured with PIV. Note that we added 500 cm^3/s to the values of Q_w measured with PIV to account for the fact that these measurements were taken from $z_1 = 4.5$ cm above the nozzle exit [see Fig. 14(a)]. Some discrepancy between these techniques was expected because the measurements with the anemometer were taken when the bubble plumes were in a straight vertical position while the measurements with PIV were averaged over 5 min, which also included the effects of wandering motion. The cumulative entrainment rates obtained here were about 30% higher than those obtained by Iguchi et al. (1991) in a confined bubble plume setup for similar air flow rates and orifice diameters.

The total entrainment rates and the depth-averaged values of kinetic energy of the mean flow and turbulent kinetic energy for each experimental condition are summarized in Fig. 15. It can be seen that the use of the airstone increases the entrainment rate by about 60% and the kinetic energy of the mean flow and turbulent kinetic energy by about 60 and 80%, respectively, when compared to the use of the multiple orifice nozzle of 4×1.5 mm. The results for the multiple orifice nozzle of 9×1.0 mm are comparable to those for the airstone, which confirms the suitability of its use for systems susceptible to rapid clogging of porous nozzles. Although the single orifice nozzle of 0.6 mm induced lower entrainment rates than the multiple orifice nozzle of 9×1.0 mm, it

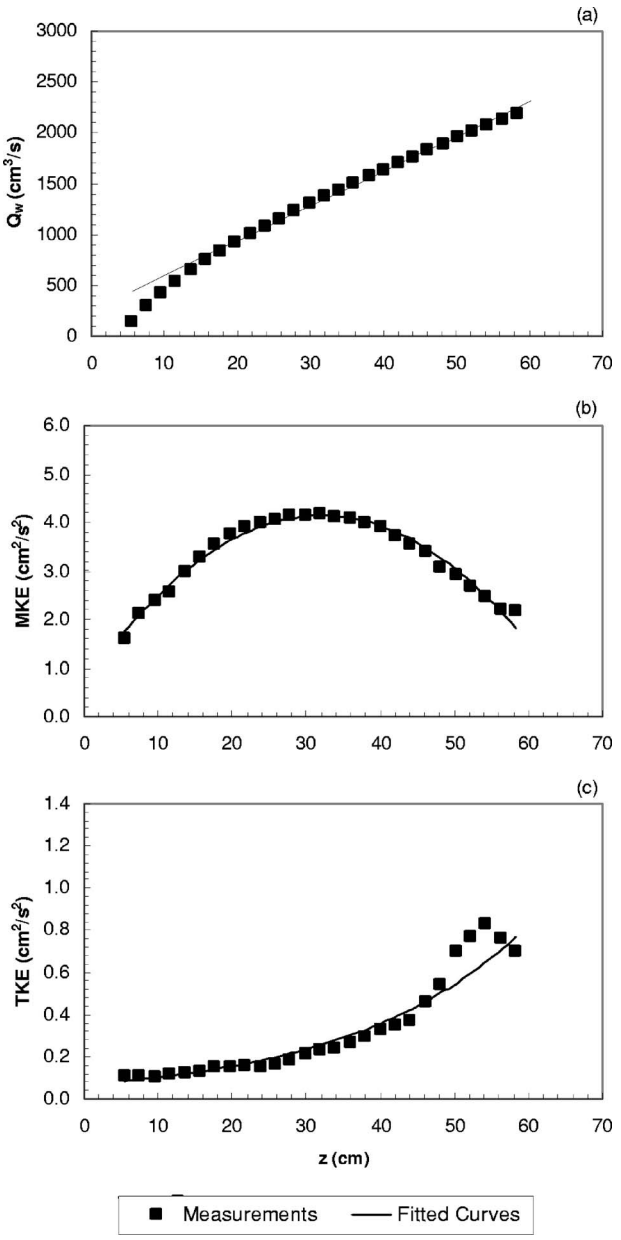

Fig. 14. Typical axial variation of: (a) cumulative entrainment rate; (b) kinetic energy of mean flow; and (c) turbulent kinetic energy (nozzle type: 9×1.0 mm, $Q_a = 33.3$ cm^3/s). Measurements shown were taken at $r = 10.8$ cm.

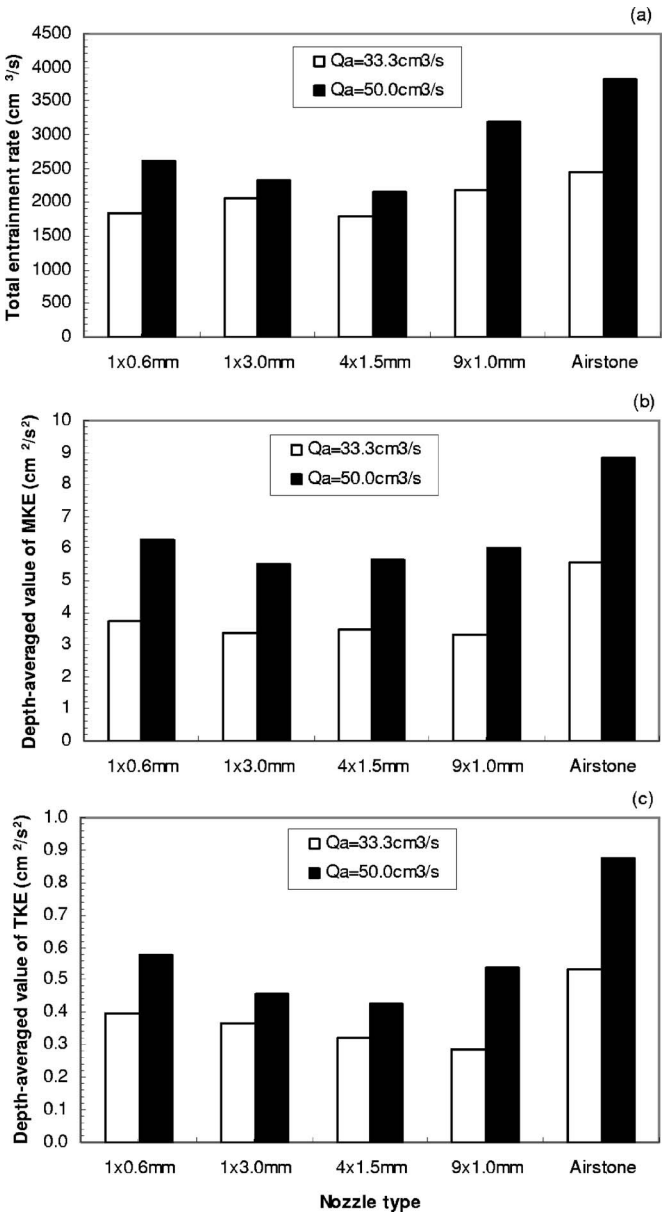

Fig. 15. (a) Total entrainment rate; (b) depth-averaged value of kinetic energy of mean flow; and (c) depth-averaged value of turbulent kinetic energy. Measurements shown were taken at $r = 10.8$ cm.

presented higher kinetic energy of the mean/turbulent flow than all the other nonporous nozzles because of the high momentum added to the flow due to the high-velocity jet. These results differ from those of Iguchi et al. (1989, 1992), who found that the mean velocity and the magnitude of the turbulent fluctuations at the bubble core centerline were independent of single orifice diameter in a confined bubble plume setup.

Similarly to the analysis for bubble characteristics, dimensional analysis gives the following relation to describe the axial variations of Q_w, MKE, and TKE for a specific distance from the bubble core

$$\left[\frac{Q_w}{Q_a}, \frac{(\text{MKE})^{0.5}}{U}, \frac{(\text{TKE})^{0.5}}{U}\right] = f\left[\frac{z}{L}, \text{F}\right] \tag{11}$$

Again, we neglected F and obtained the following dimensionless correlations by adjusting a straight line, a polynomial curve, and an exponential curve to the axial variations of Q_w, MKE, and TKE, respectively, the variation corresponding approximately to the upper and lower limits obtained with different nozzles

$$\frac{Q_w}{Q_a} = 3 + (1.15 \pm 26\,\%)\left(\frac{z}{L}\right) \tag{12}$$

$$\frac{(\text{MKE})^{0.5}}{U} = -5x10^{-5}\left(\frac{z}{L}\right)^2 + 0.0031\left(\frac{z}{L}\right) + (0.03 \pm 45\,\%) \tag{13}$$

$$\frac{(\text{TKE})^{0.5}}{U} = (0.014 \pm 40\,\%)e^{0.013(z/L)} \tag{14}$$

Fig. 16 shows a reasonably good correlation of Eqs. (12)–(14) to experimental data. The upper and lower limits represented by

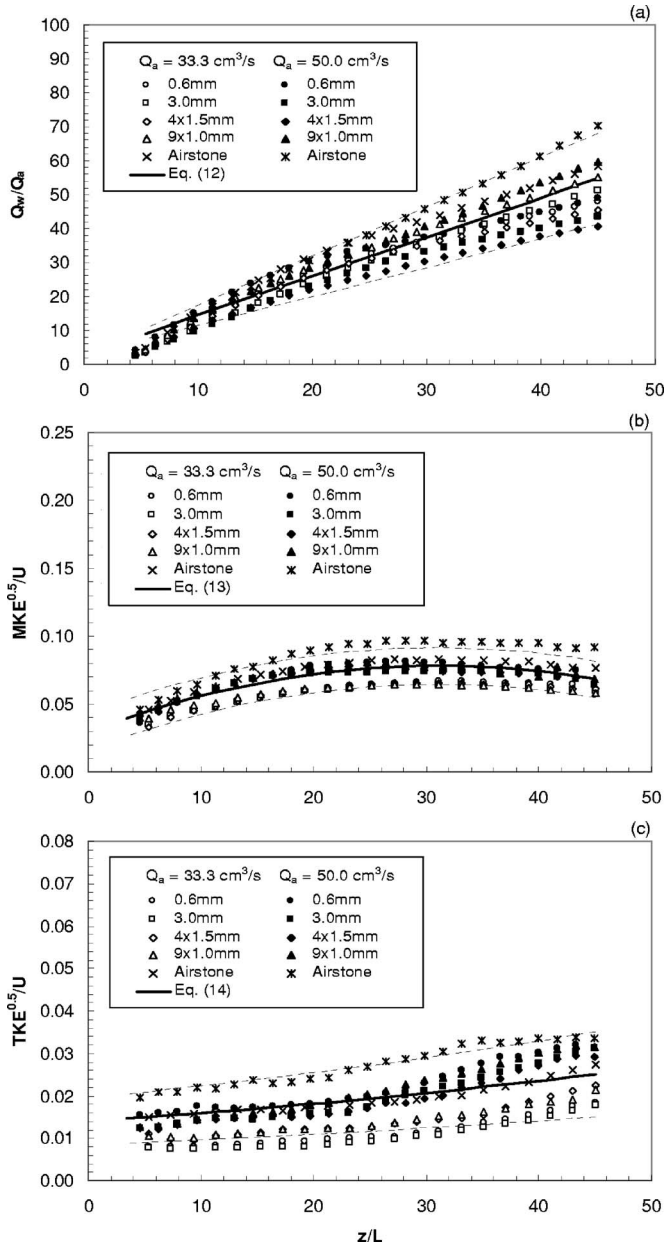

Fig. 16. Adjustment of Eqs. (12)–(14) to experimental data, with dashed lines indicating approximately maximum variation of each parameter with nozzle type

dashed lines clearly show the maximum variation of each parameter with nozzle type (e.g., dimensionless entrainment rate increases when using the porous airstone instead of the multiple orifice nozzle of 4×1.5 mm). The results also confirm that the effects of F are relatively small for our experimental conditions.

Applications

The above results can be used to compare the aeration potential of air injection with different nozzles in shallow wastewater tanks and rivers. An example would be the use of mean bubble diameter and interfacial area to estimate the volumetric mass transfer coefficient (K_La) for each nozzle. Table 1 presents estimations of this coefficient considering the correlation given by Wüest et al. (1992) and McGinnis and Little (2002) for K_L as a function of the mean bubble diameter. The values of K_La ranged from 8.65 h^{-1} for the single orifice nozzle of 3.0 mm to 19.16 h^{-1} for the porous airstone, and are within the range from 0.12 h^{-1} for coarse bubble diffusers to 40.15 h^{-1} for very fine bubble diffusers obtained by Schierholz et al. (2006). This suggests that the nozzles evaluated in this study behaved similarly to their fine bubble diffusers. Note that even higher values of K_La are expected in rivers because of enhanced turbulence and bubble breakup processes due to the effect of crossflow. Since the K_La values due to bursting of bubbles at the water surface obtained by Schierholz et al. for fine bubble diffusers decreased from about 45 to 5% of those due to bubble plume aeration as the air flow rate decreased, we expect a contribution even smaller than 5% in our tests because our flow rates were much smaller.

The correlations obtained here can be applied to predict bubble characteristics and surrounding flow structure in aeration/mixing systems for air flow rates and nozzles similar to those tested in this study. An example of this application would be a bubble plume in a wastewater tank of 4 m diameter and 1.8 m depth where a circulation flow of about 30,000 cm^3/s is desired to prevent suspended solids deposition and formation of an anaerobic layer at the bottom. Thus, considering an initial surface jet thickness of about 30 cm (i.e., 1/6 of water depth, as mentioned above), the correlation given by Eq. (12) predicts an air flow rate Q_a of 415 cm^3/s to attain such a requirement. In this case, we could use a circular nozzle of 90 orifices of 1.0 mm diameter with similar flow rate per orifice as the nozzle of 9×1.0 mm tested here. Notice that this assumption is not expected to be valid for much higher flow rates per orifice because continuous bubble jets are formed and the flow pattern changes significantly, as the supersonic flow studies conducted by Kobus (1968). Similar analysis can be applied for the porous airstone, but the flow rate per unit area of the stone should be considered instead of the flow rate per orifice.

It is also important to note that, in real wastewater treatment plants, the presence of suspended solids may affect the movement and morphology of the bubbles. Although little is known about the effect of suspended solids and other impurities on bubble swarms, studies on isolated bubbles show that it results in decreased bubble slip velocities due to increased drag forces. The curve given by Clift et al. (1978) shows that the difference between bubble slip velocity in pure and contaminated water systems varies by about 30% for the range of bubble equivalent diameters of 3–12 mm obtained in our study. In this case, we expect that decreases in bubble slip velocity will decrease the turbulence levels and the induced liquid volume flux by generating wakes behind the bubbles with lower velocities (see Leitch and Baines 1989). On the other hand, we expect a counterbalancing effect of increased turbulence due to particle-particle and particle-bubble interactions. Therefore, in wastewater treatment systems, we believe that our correlation for liquid volume flux would give reasonably accurate results with an error of less than about 30% due to the presence of suspended solids in the water.

This study also provides information such as bubble size distribution and entrainment rate for initial conditions in integral bubble plume models (see Wüest et al. 1992) and turbulent flow structure for evaluation and validation of computational fluid dynamics models for more detailed analysis of bubble plume systems (see Buscalia et al. 2002). Besides information on surface jet thickness and flow rate can be applied to estimate surface aeration due to turbulent diffusion (see Chu and Jirka 2003).

Summary and Conclusions

An experimental study on air injection in a relatively large water tank was performed to investigate the effect of nozzle type, including single/multiple orifice nozzles and a porous airstone, on the characteristics of the bubbles and the surrounding liquid flow structure. The results revealed that radial distributions of bubble size and velocity were well described by a straight line, while the specific interfacial area followed a Gaussian curve. Bubble slip velocity was found to be higher than the terminal bubble velocity obtained from the literature for isolated bubbles. The water velocity within the bubble plume was found to decrease linearly from the center of the plume to close to zero at the edge of the plume. The variation of cumulative liquid entrainment rate with height was well described by a straight line, while the variations of kinetic energy of the mean flow and turbulent kinetic energy near the bubble core were well described by a polynomial curve and an exponential curve, respectively.

Although bubble velocity did not change significantly, bubble mean Sauter diameter could be decreased by about 50% while air-water specific interfacial area could be increased by about 90% by using the porous airstone instead of a single orifice nozzle of 3.0 mm diameter. The use of the airstone could also increase the liquid entrainment rate by about 60% and the kinetic energy of the mean and turbulent flow near the bubble core by about 60 and 80%, respectively. The results for a nozzle with nine orifices of 1.0 mm diameter are comparable to those for the airstone, which suggests the suitability of nozzles with multiple orifices of small diameter for systems susceptible to clogging of porous nozzles such as wastewater treatment tanks and natural water bodies with a high concentration of suspended solids and/or organic matter.

Dimensionless correlations using length and velocity scales based on the air flow rates described well the radial variations of the bubble properties and the axial variations of the entrainment rate and kinetic energy of the mean flow and turbulent kinetic energy near the bubble core, and are suggested here for design purposes of artificial aeration/mixing systems. Finally, applications of the results such as estimation of the volumetric mass transfer coefficient and entrainment rate for different artificial aeration/mixing systems are presented.

Acknowledgments

The first writer is supported by the Coordination for the Improvement of Higher Education Personnel Foundation (CAPES), Ministry of Education, Brazil. The writers are grateful to Perry Fedun and Chris Krath for building the experimental apparatus.

Notation

The following symbols are used in this paper:

a = air-water specific interfacial area (m^{-1});
C = dissolved oxygen (DO) concentration in water (mg/L);
C_s = saturation DO concentration in water (mg/L);
d_b = bubble mean Sauter diameter (mm);
f_b = bubble frequency (Hz);
L = length scale defined by $L=(Q_a^2/g)^{1/5}$ (cm);
MKE = kinetic energy of the mean flow (cm^2/s^2);
Q_a = volumetric air flow rate (cm^3/s);
Q_w = volumetric entrainment rate (cm^3/s);
r = radial distance from plume centerline (cm);
TKE = turbulent kinetic energy (cm^2/s^2);
U = velocity scale defined by $U=Q_a/L^2$ (cm/s);
u_b = bubble velocity (m/s);
$\overline{u'u'}$ = horizontal normal stress due to turbulent fluctuations (cm^2/s^2);
$\bar{u}$, $\bar{v}$ = time-averaged horizontal and vertical velocity component (cm/s);
$\overline{u'v'}$ = shear stress due to turbulent fluctuations (cm^2/s^2);
u', v' = turbulent horizontal and vertical velocity fluctuation (cm/s);
u'', v'' = periodic horizontal and vertical velocity fluctuation (cm/s);
$\overline{v'v'}$ = vertical normal stress due to turbulent fluctuations (cm^2/s^2);
z = axial distance from the nozzle exit (cm); and
α = air concentration or void fraction (%).

References

ASCE. (2007). "Measurement of oxygen transfer in clean water." *ASCE/EWRI 2-06*, Reston, Va.

Barnhart, E. L. (1969). "Transfer of oxygen in aqueous solutions." *J. Sanit. Engrg. Div.*, 95(3), 645–661.

Boes, R. M., and Hager, W. H. (2003). "Two-phase flow characteristics of stepped spillways." *J. Hydraul. Eng.*, 129(9), 661–670.

Boyer, C., Duquenne, A. M., and Wild, G. (2002). "Measuring techniques in gas-liquid and gas-liquid-solid reactors." *Chem. Eng. Sci.*, 57(16), 3185–3215.

Brücker, C., and Schröder, W. (2004) "PIV-study on bubble interaction and wakes in multiphase flows." *Bubbly flows-Analysis, modelling and calculation*, M. Sommerfeld, ed., Springer, Berlin.

Buscalia, G. C., Bombardelli, F. A., and García, M. H. (2002). "Numerical modeling of large-scale bubble plumes accounting for mass transfer effects." *Int. J. Multiphase Flow*, 28(11), 1763–1785.

Chang, K. A., Lim, H. J., and Su, C. B. (2003). "Fiber optic reflectometer for velocity and fraction ratio measurements in multiphase flows." *Rev. Sci. Instrum.*, 74(7), 3559–3565.

Chanson, H. (1997) "Measuring air-water interface area in supercritical open channel flow." *Water Res.*, 31(6), 1414–1420.

Chaumat, H., Billet-Duquenne, A. M., Augier, F., Mathieu, C., and Delmas, H. (2005). "Application of the double optic probe technique to distorted tumbling bubbles in aqueous or organic liquid." *Chem. Eng. Sci.*, 60(22), 6134–6145.

Chu, C. R., and Jirka, G. H. (2003). "Wind and stream flow induced reaeration." *J. Environ. Eng.*, 129(12), 1129–1136.

Clift, R., Grace, J. R., and Weber, M. E. (1978). *Bubbles, drops and particles*, Academic, New York.

DeMoyer, C. D., Schierholz, E. L., Gulliver, J. S., and Wilhelms, S. C. (2003). "Impact of bubble and free surface oxygen transfer on diffused aeration systems." *Water Res.*, 37(8), 1890–1904.

Eckenfelder, W. W. (1959). "Absorption of oxygen from air bubbles in water." *J. Sanit. Engrg. Div.*, 85(4), 89–99.

Fanneløp, T. K., Hirschberg, S., and Küffer, J. (1991). "Surface current and recirculating cells generated by bubble curtains and jets." *J. Fluid Mech.*, 229, 629–657.

Friedl, M. J., and Fanneløp, T. K. (2000). "Bubble plumes and their interaction with the water surface." *Appl. Ocean. Res.*, 22(2), 119–128.

García, C. M., and García, M. H. (2006). "Characterization of flow turbulence in large-scale bubble-plume experiments." *Exp. Fluids*, 41(1), 91–101.

Iguchi, M., Nozawa, K., Tomida, H., and Morita, Z. (1992). "Bubble

characteristics in the buoyancy region of a vertical bubbling jet." *ISIJ Int.*, 32, 747–754.
Iguchi, M., Takeuchi, H., and Morita, Z. (1991). "The flow field in air-water vertical bubbling jets in a cylindrical vessel." *ISIJ Int.*, 31, 246–253.
Iguchi, M., Tani, J., Uemura, T., Kawabata, H., Takeuchi, H., and Morita, Z. (1989). "The characteristics of water and bubbling jets in a cylindrical vessel with bottom blowing." *ISIJ Int.*, 29, 309–317.
Kiambi, S. L., Duquenne, A. M., Dupont, J. B., Colin, C., Risso, F., and Delmas, H. (2003). "Measurements of bubble characteristics: Comparison between double optical probe and imaging." *Can. J. Chem. Eng.*, 81(3–4), 764–770.
Kiger, K. T., and Pan, C. (2000). "PIV technique for the simultaneous measurement of dilute two-phase flows." *J. Fluids Eng.*, 122(4), 811–818.
Kobus, H. (1968). "The motion of bubbles in liquids." *Characteristics of self-aerated free-surface flows, Water and waste water—Current research and practice*, L. Rao and H. Kobus, eds., Vol. 10, Erich Schimidt Verlag, Berlin.
Leitch, A. M., and Baines, W. D. (1989). "Liquid volume flux in a weak bubble plume." *J. Fluid Mech.*, 205, 77–98.
Lima Neto, I. E., Zhu, D. Z., and Rajaratnam, N. (2007a). "Effect of tank size and geometry on the flow induced by circular bubble plumes and water jets." *J. Hydraul. Eng.* in press.
Lima Neto, I. E., Zhu, D. Z., Rajaratnam, N., Yu, T., Spafford, M., and McEachern, P. (2007b). "Dissolved oxygen downstream of an effluent outfall in an ice-covered river: Natural and artificial aeration." *J. Environ. Eng.*, 133(11), 1051–1060.
McCord, S. A., Schladow, S. G., and Miller, T. G. (2000). "Modeling artificial aeration kinetics in ice-covered lakes." *J. Environ. Eng.*, 126(1), 21–31.
McGinnins, D. F., and Little, J. C. (2002). "Predicting diffused-bubble oxygen transfer rate using the discrete-bubble model." *Water Res.*, 36(18), 4627–4635.
McGinnis, D. F., Lorke, A., Wüest, A., Stockli, A., and Little, J. C. (2004). "Interaction between a bubble plume and the near field in a stratified lake." *Water Resour. Res.*, 40(10), W10206.
McWhirter, J. R., and Hutter, J. C. (1989). "Improved oxygen mass transfer modeling for diffused/subsurface aeration systems." *AIChE J.*, 35(9), 1527–1534.
Motarjemi, M., and Jameson, G. J. (1978). "Mass transfer from very small bubbles—The optimum bubble size for aeration." *Chem. Eng. Sci.*, 33(11), 1415–1423.
Mueller, J. A., Boyle, W. C., and Pöpel, H. J. (2002). *Aeration: Principles and practice*, CRC, New York.
Murzyn, F., Mouaze, D., and Chaplin, J. R. (2005). "Optical fibre probe measurements of bubbly flow in hydraulic jumps." *Int. J. Multiphase Flow*, 31(1), 141–154.
Rensen, J., and Roig, V. (2001). "Experimental study of the unsteady structure of a confined bubble plume." *Int. J. Multiphase Flow*, 27(8), 1431–1449.
Riess, I. R., and Fanneløp, T. K. (1998). "Recirculation flow generated by line-source bubble plumes." *J. Hydraul. Eng.*, 124(9), 932–940.
Rosso, D., and Stenstrom, M. K. (2006). "Surfactant effects on alpha-factors in aeration systems." *Water Res.*, 40(7), 1397–1404.
Ruzicka, M. C. (2000). "On bubbles rising in line." *Int. J. Multiphase Flow*, 26(7), 1141–1181.
Sahoo, G. B., and Luketina, D. (2006). "Response of a tropical reservoir to bubbler destratification." *J. Environ. Eng.*, 132(7), 736–746.
Schierholz, E. L., Gulliver, J. S., Wilhelms, S. C., and Henneman, H. E. (2006). "Gas transfer from air diffusers." *Water Res.*, 40(5), 1018–1026.
Soga, C. L. M., and Rehmann, C. R. (2004). "Dissipation of turbulent kinetic energy near a bubble plume." *J. Hydraul. Eng.*, 130(5), 441–449.
Swan, C., and Moros, A. (1993). "The hydrodynamics of a subsea blow-out." *Appl. Ocean. Res.*, 15(2), 269–280.
Toombes, L., and Chanson, H. (2005). "Air-water mass transfer on a stepped waterway." *J. Environ. Eng.*, 131(10), 1377–1386.
Wain, D. J., and Rehmann, C. R. (2005). "Eddy diffusivity near bubble plumes." *Water Resour. Res.*, 41(9), W09409.
Water Pollution Control Federation (WPCF). (1988). *Aeration—Manual of practice*, No. FD-13, Alexandria, Va.
Wüest, A., Brooks, N. H., and Imboden, D. M. (1992). "Bubble plume modeling for lake restoration." *Water Resour. Res.*, 28(12), 3235–3250.